

Investigation on Be, Mg, Ca, B, Ga, C, Si, and Ge atoms doped on Al (111) surface and their effect on oxygen adsorption: A first-principle calculation[☆]

Liang Junxi^{a,*}, Qi Bomiao^{a,b}, Lu Mengmeng^a, Zhou Yaoyu^a, Ren Fang^a, Shen Yan^b, Li Guihua^a, Pang Shaofeng^a, Wang Yanbin^a, Su Qiong^{a,*}

^a Key Laboratory of Environment-Friendly Composite Materials of the State Ethnic Affairs Commission, Gansu Province Engineering Research Center for Biomass Functional Composite Materials, Key Laboratory for the Utilization of Environment-Friendly Composite Materials and Biomass in Universities of Gansu Province, Gansu Province Research Center for Basic Sciences of Surface and Interface Chemistry, College of Chemical Engineering, Northwest Minzu University, Lanzhou, Gansu 730030, PR China

^b College of Materials Science and Engineering, Nanjing Tech University, Nanjing 211800, PR China



ARTICLE INFO

Keywords:

Al (111) surface
Doping atom
Adsorbing oxygen
First-principle calculation

ABSTRACT

Oxygen corrosion of the aluminum alloy has a substantial impact on the durability of engineering materials and equipment. To better understand how various alloy elements affect oxygen corrosion, we used first-principle DFT method to study the role of each given dopant atom (Be, Mg, Ca, B, Ga, C, Si, and Ge) in the formation of surface oxide film on the Al (111) surface, in the case replacing a surface Al atom. Our calculations show that the electron gain or loss abilities of these alloy elements differ from that of Al metal, with Be, B, C, and Si atoms tending to penetrate into the surface, Mg, Ca, and Ga atoms protruding, and Ge atom just embedded into the Al (111) surfaces. Additionally, the type of doping element at the Al (111) surface can greatly affect the O₂ absorption, predicting that Ca-doped surface absorb the least amount of oxygen, followed by Si-doped surface, with Be-, Mg-, B-, Ga-, C-, and Ge-doped surfaces showing higher O₂ absorption. Based on adsorption energy (E_{ads}) and partial density of states (PDOS) analysis, we conclude that the doped Al (111) surfaces can make O₂ adsorption different owing to the difference in electronic properties of the doping atoms. These insights draw a greater knowledge of the role of alloy elements in the oxygen corrosion of Al alloys, enabling guidance for designing more corrosion-resistant materials.

1. Introduction

Aluminum (Al) alloys usually have high specific strength, excellent formability, good heat dissipation, and corrosion resistance. Therefore, their application and research are very extensive. [1] Aside from the wide range of experimental investigations, a large number of simulations have been also used to study the properties of various Al alloys. As early as 1994 Jin et al. [2] utilized the cluster theory to explore the interaction of water with Al (111) surface under low surface coverage, revealing significant adsorption-induced surface relaxation effects. In their results the considerable relaxation effects are found although, unlike for the adsorbate geometry, the substrate geometries do not converge rapidly with cluster size. Furthermore, the first-principles calculations were carried out to investigate the co-adsorption of H₂O

and O₂ on the surface of Al (111), [3] proposing that a pre-adsorbed O atom can promote the dehydrogenation reaction of H₂O. However, as we all know, the acidifying, alkalinizing, oxidizing and so on corrosion resistance of metallic Al is relatively poor, thereby necessitating the appropriate treatment. Most of the earlier research tended to develop a corrosion-resistant coating to improve the ability of aluminum to resist corrosion. Cao et al. prepared a TiC martensitic stainless steel (TiC/MSS) composite coating on the Al surface using a new method of circular oscillating laser, which successfully improved the Al's corrosion resistance. [4] Similarly, Li et al. [5] improved the corrosion resistance of the 6N01 Al alloy by preparing layered double hydroxide (LDH) films composed of lithium (Li) and Al elements. Chen et al. [6] took advantage of the anodized alumina-copper (Al-Cu) coating on Al substrate to achieve outstanding antimicrobial properties and mechanical stability.

[☆] Project supported: Fundamental Research Funds for the Central Universities (31,920,220,063, 31,920,240,125–06), the National Natural Science Foundation of China (22,165,025, 22,262,031), Chemistry Discipline Innovation Team of Northwest Minzu University (1,001,660,139, 1,001,660,141).

* Corresponding authors.

E-mail addresses: xbmujxliang@126.com (L. Junxi), hgsq@xbmu.edu.cn (S. Qiong).

Of course, there were numerous DFT studies about the corrosion resistance of Al alloys, such as molecular modelling framework of metal-organic clusters for conserving surfaces, [7] molecular simulation of Al-Ga surface garnished with chromium for organic material detection, [8] examination of aluminum-based nanocluster alloys shielded by nitrogen heterocyclic carbenes as corrosion inhibitors, [9] and investigation of aluminum lattice nanoclusters protected by organic inhibitor coatings [10]. It is noteworthy that the addition of minor amounts of some elements, such as Si, Ag, Mn, Zn, Ge, and Sn, has been reported to have a substantial effect on the microstructure evolution and heat treatment response of Al metal [11-20]. In contrast, there has been limited research into the effect of some elements' doping on the surface oxidation process, especially little systematical studying influences of the neighbour elements. This is a very meaningful and important scientific topic, which will have a tremendous influence on the structural design and performance improvement of aluminum alloys.

The oxidation of metallic Al and its alloys has greatly attracted the attention of researchers and been studied both experimentally and computationally [21-23]. In general, the oxidation of the clean Al and Al-based alloy can achieve themselves protection against corrosion by forming an oxide film on their surfaces. Kim et al. [24] used *ab initio* molecular dynamics simulations to investigate the growth and properties of oxide films on the Al (100), (110), and (111) surfaces, demonstrating that the film formation involves dissociative of O₂ on the surfaces, migration of O atoms on the surfaces, and subsequent oxide formation. They also confirmed experimentally that Al (100) has a slower film forming rate than Al (111). Additionally, Cai et al. [25] used X-ray photoelectron spectroscopy (XPS) to study the degree of oxidation on the Al surface at room temperature and discovered that the oxide film on the surface becomes thicker with the increase of oxygen partial pressure. However, many researchers have proposed the oxidation resistance of the Al surface can be improved by altering the doping components. Recently, Qiao et al. [26] investigated the adsorption and dissociation of oxygen on M-doped (M = Cu, Ag, W) Al (111) surfaces using density functional theory (DFT), indicating that Cu and Ag-doped surfaces are more easily oxidized than W-doped surface. Furthermore, Ji et al. [27] used first-principles simulations to study the effects of Zn, Mg, and Cu doping on Al (111) surfaces, proposing that Zn and Mg hinder the oxidation reaction of Al surfaces. As a result, the effect of different elements doped surface on oxidation process remains to be examined systematically. Such a comprehensive investigation should be both academically rewarding and practical implications. Moreover, properties can be better understood by looking at trends among substituents or examining systems with elements from the same period or group. For example, Monajjemi et al. [28] investigated transition metal (X = Mn, Fe, Co, Ni, Cu, Zn)-doped graphene (C-NG) as gas sensor for CO₂ and NO₂ detection, illustrating a more significant charge transfer for Ni-doped C-NG through CO₂ adsorption and a more remarkable charge transfer for Co-doped C-NG via NO₂ adsorption. Furthermore, they have also studied high selectivity of atom-doped on boron nitride nanocage for gas molecules adsorption and found the order of Cu > Co > Cr > V > Zn > Sc. [29] For the purpose stated above, in this paper the effects of doping elements such as Be, Mg, Ca, B, Ga, C, Si, and Ge on the oxidation of the Al (111) surface were investigated in detail, in which the dopant atom substitutes an Al (111) surface atom—building a plane doped Al (111) surface with a substitutional atom. The goal of this study is to evaluate how various dopants affect Al (111) surface oxidation, aiming to identify advantageous components for promoting oxidation. Furthermore, related research results will provide a better knowledge of oxidation and protection mechanisms in the surface and interface of the Al-based alloys and offers new insights for future design and synthesis of these materials.

2. Computational methods

All the calculations were performed in Materials Studio 8.0 using

Cambridge Serial Total Energy Package (CASTEP) code, which is based on the density functional theory (DFT) method with a plane wave basis set and using pseudopotentials. [30] The exchange-correlation energy was calculated using the gradient corrected generalized gradient approximation (GGA) approach with the Predew-Buekew-Ernzerhn (PBE) functional [31], which provided a good description of the electronic properties and structures of metal materials and their surfaces [32-35]. To test the validity of our selected method, we calculated the lattice parameters of the bulk Al using the bcc symmetric 3D pristine cells. The obtained value of 4.257 Å closely matched both the experimental value of 4.050 Å [36] and theoretical value of 4.081 Å [37]. On the basis of the full relaxation, we firstly created an Al crystal (111) plane and then built a 3 × 3 surface model with four-layer slabs. Within these layers, different Al alloy configurations were constructed by individually replacing an Al atom in the top layer with Be, Mg, Ca, B, Ga, C, Si, and Ge atoms. According to previous published work [38], for those configurations the structural relaxation was allowed for the top three layers while the bottom layer remained fixed, and a vacuum region measuring 15 Å was placed perpendicular to the surface, which can obtain more accurate and rational surface properties. In our calculations, the cutoff energy of 450 eV was employed for plane wave expansions. The Brillouin zone is sampled by using a 5 × 5 × 1 grid. [39] The DFT + *D* (dispersion) calculation corrected the van der Waals's force. [40] The self-consistent field cycle convergence criterion was 1.0 × 10⁻⁵ eV, with all atoms experiencing forces of <0.03 eV/Å. The maximum stress and displacement were 0.05 GPa and 0.001 Å, respectively. Furthermore, using the Langmuir adsorption model at the one-layered Integrated molecular Orbital and molecular Mechanics (ONIOM) levels of theory [41], we examined the O₂ adsorption on both doped and clean Al (111) surfaces, in which the above constructed 3 × 3 pure and doped Al surface super cells were used to adsorb O₂ molecule. The related configurations can be found in Figs. 1, 2, and 3 of the Supporting Material.

Surface energy (γ_{surf}) measures surface stability, with lower values indicating better stability [42]. Based on the formula of the γ_{surf} for clean γ -TiAl, [43] In this study the γ_{surf} for the pure/doped Al system can be written as:

$$\gamma_{\text{surf}} = \frac{E_{\text{unrelax}} - \sum n_i u_i}{2A} + \frac{E_{\text{relax}} - E_{\text{unrelax}}}{A} \quad (1)$$

Where E_{unrelax} is the total energy of the surface model before optimization, E_{relax} is the total energy of surface model after optimization, $\sum n_i u_i$ is the total energy of the surface atoms in the bulk phase, n_i is the total number of atoms in surface model, u_i is the energy of one atom in a single crystal, and A is the surface area.

The binding energy (E_b) of the doping atoms reported herein is obtained as [44]:

$$E_b = \frac{E_{\text{slab}} - (n - m)E_{\text{Al}} - mE_M}{n + m} \quad (2)$$

Where E_{slab} is the total energy of the pure/doped Al surface, n and m denote the total number of Al and doped atoms, respectively, E_{Al} and E_M are the bulk energy per unit atom of Al and doped atoms, respectively. Here, the E_{Al} and E_M calculations induced from that the bulk energy divided by the total number of atoms in the bulk.

The adsorption energy (E_{ads}) is calculated by the following expression.

$$E_{\text{ads}} = E_{\text{ad+surf}} - E_{\text{ad}} - E_{\text{surf}} \quad (3)$$

In the formula, $E_{\text{ad+surf}}$, E_{ad} and E_{surf} are the total energies of an O-adsorbed pure/doped Al surface, a clean pure/doped Al surface and an isolated O₂ molecule, respectively. Based on this equation, a negative E_{ads} value suggests an exothermic adsorption process, and the smaller the value, the stronger the interaction between the adsorbate and the surface [45].

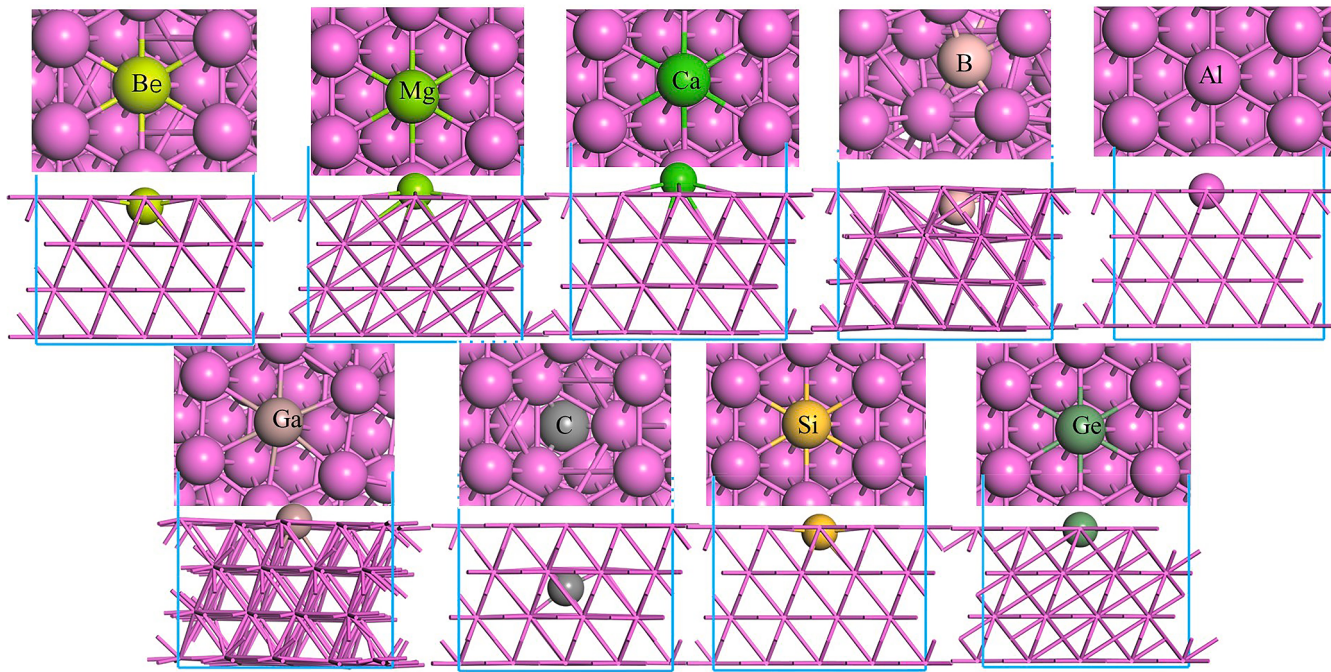


Fig. 1. Optimized configurations of the pure and doping Al (111) surfaces.

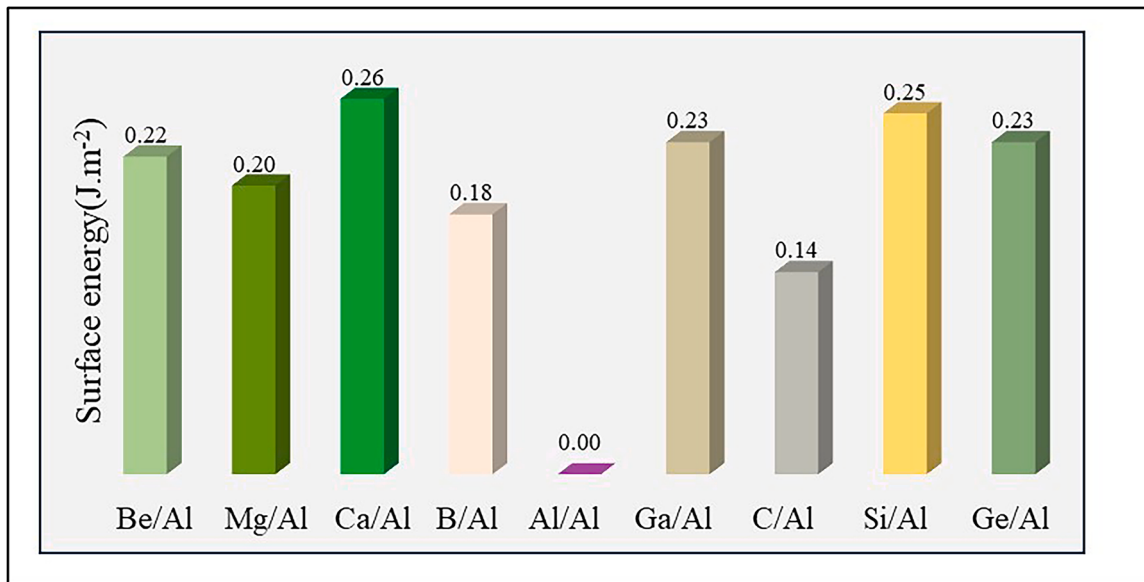


Fig. 2. Surface energy of the doped Al (111) surfaces compared to the pure Al (111) surface.

3. Results and discussions

3.1. Surface analysis

To investigate the effect of the doped elements on the Al (111) surface binding and stability, eight surface doping models were constructed by replacing one Al atom of the first layer with the Be, Mg, Ca, B, Ga, C, Si, and Ge atoms, respectively. In this research the pure Al (111) surface model was marked as “pure Al”, while the other eight atoms-doped Al (111) surface models were labeled as Be/Al, Mg/Al, Ca/Al, B/Al, Ga/Al, C/Al, Si/Al, and Ge/Al, respectively. Geometries of the constructed surface configurations were relaxed to the external and internal degrees of freedom through DFT structural optimization until the force and stress vanished. The fully relaxed surface configurations before and after

doping with Be, Mg, Ca, B, Ga, C, Si and Ge atoms are depicted in Fig. 1. Upon comparing the Be/Al, Mg/Al, Ca/Al, B/Al, Ga/Al, C/Al, Si/Al, and Ge/Al configurations, it was discovered that the doping C, Be, Si, and B atoms penetrated into the Al (111) surface to a different depth because of different atomic radius, the Mg, Ca, and Ga atoms obviously protruded from Al (111) surface, and only the Ge atom just embedded into the Al (111) surface. The average bond lengths (\AA) of Be-Al, Mg-Al, Ca-Al, B-Al, Al-Al, Ga-Al, C-Al, Si-Al, and Ge-Al bonds in the first layer of the surfaces were measured as 2.89, 3.09, 3.23, 2.29, 3.01, 3.03, 2.07, 2.98, and 3.08, respectively, as listed in Table 1. Obviously, compared to the Al-Al bond length of 3.01 \AA , the C-Al bond exhibited the shortest distance at 2.07 \AA , which means that the C doping atom makes the surrounding Al atoms greatly attracted to them. Especially, it also found that C-doped surface had the most deeply embedded C atom in the

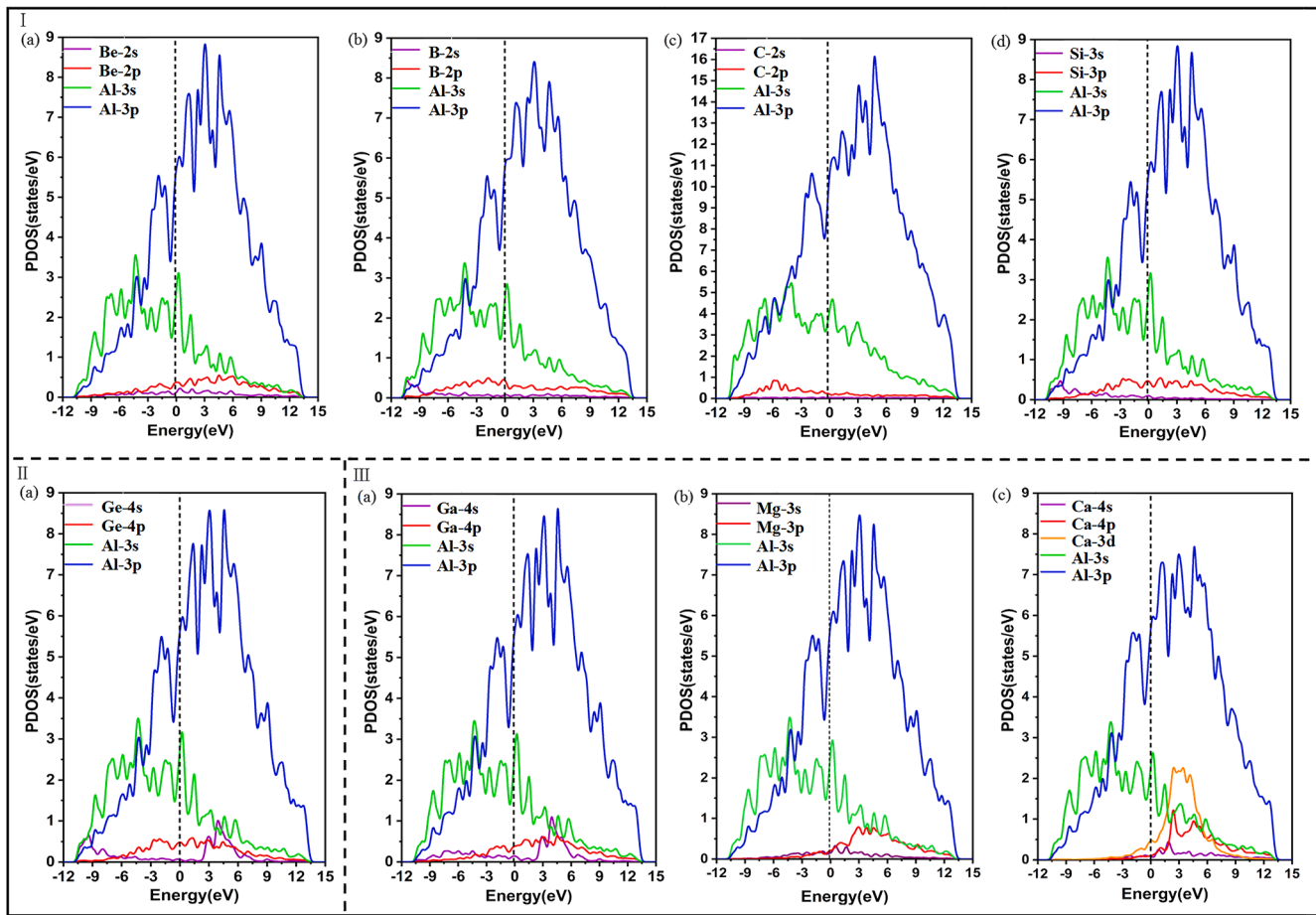


Fig. 3. PDOS of the O₂ adsorption on the doping Al (111) surfaces. Regions I, II, and III reflect the PDOS of the penetrated, the embedded, and the protruded doping arrangements, respectively.

Table 1

Average bond length, COOP, and COHP of the dopant elements bound to the adjacent Al atoms on the Al (111) surfaces.

Species	Average bond length (Å)	COOP (eV)	COHP (eV)
Be/Al	2.89	-2.99	1.09
Mg/Al	3.09	-1.63	0.54
Ca/Al	3.23	-1.90	0.27
B/Al	2.29	-5.44	2.18
Ga/Al	3.03	-2.72	0.54
C/Al	2.07	-5.17	1.36
Si/Al	2.98	-1.63	0.27
Ge/Al	3.08	-1.90	0.27
pure Al	3.01	-2.72	0.82

structure. Thus, the incorporation of C atom should have less effect on the energy stability of the Al (111) surface.

The binding energy (E_b) serves to assess the strength of the bonding per doping atom with Al atoms. The corresponding E_b values are listed in **Table 2**. It is clearly seen that all doping atoms can be stably combined with Al atoms owing to the negative E_b values. The Mg-doped surface exhibited the lowest E_b of -0.95 eV, while the Ca-doped surface showed the highest E_b of -0.92 eV, so the doping atoms will enhance the bonding between the atoms on the Al (111) surface. Meanwhile, as shown in **Table 1**, analysis of both crystal orbital occupies populations (COOP) and crystal orbital Hamilton populations (COHP) values reveals a consistent trend for the nine studied systems, all implying strong bonding between surface atoms, thereby enhancing the energy stability of the doped Al surfaces. In this paper we chose COHP analysis to explain

Table 2

The calculated binding energy (E_b), surface energy (γ_{surf}), and charges transfer for the Al (111) surface doping models.

Species	E_b /eV	γ_{surf} /J·m ⁻²	charges transfer/e ^a
Be/Al	-0.94	1.80	-0.34
Mg/Al	-0.95	1.78	0.74
Ca/Al	-0.94	1.84	0.75
B/Al	-0.93	1.76	-1.01
Ga/Al	-0.94	1.81	-0.04
C/Al	-0.92	1.72	-1.25
Si/Al	-0.94	1.83	-0.21
Ge/Al	-0.94	1.81	-0.07

^a charge transfer was calculated by Mulliken analysis and the corresponding value is the charge difference of the doped atom before and after doping.

bond strength between Al and doped atoms. As shown in **Table 1**, compared with COHP (eV) of the Al-Al bond (0.82), the Mg-Al (0.54), Ca-Al (0.27), Ga-Al (0.54), Si-Al (0.27) and Ge-Al (0.27) bonds strength decreased, while Be-Al (1.09), B-Al (2.18) and C-Al (1.36) bonds strength increased. This result mainly derived from the radius and electronic properties of the doping atoms. **Table 2** shows that surface energies (γ_{surf}) values of all doped surfaces are positive, helping to surface adsorption. For the γ_{surf} of the pure Al (111) surface, our GGA-PBE calculated value (1.58 J·m⁻²) is lower than the GGA/PW91 calculations (2.791 J·m⁻²), [26] which derived from GGA/PW91 functional overestimates the unbond energy, however, our result is well-matched with experimental value of 1.16 J·m⁻², [46] although it is somewhat high by comparison. Moreover, as may be seen from **Fig. 2**, the doped surfaces

exhibit greater γ_{surf} values compared to the pure Al surface, which is in good agreement with Qiao et. al's findings [26]. That means that the doping atoms are more favorable for small molecules. Our finding illustrates the relative γ_{surf} ($\text{J}\cdot\text{m}^{-2}$) tendency as pure Al (0.00) < C/Al (0.14) < B/Al (0.18) < Mg/Al (0.20) < Be/Al (0.22) < Ge/Al (0.23) = Ga/Al (0.23) < Si/Al (0.25) < Ca/Al (0.26), thereby the surface activity after doping becomes stronger, with the Ca-atom doped surface having the maximum activity. It is believed that Ca-doped Al surface is very rapidly corroded by oxidation. In fact, from our studying the O_2 adsorption on the Ca-atom doped surface is very poor, with weak physical adsorption as the major interaction mechanism. To this point, we examined the charge transfer calculated by Mulliken analysis on the Ca-doped surface. As reported in Table 2, the Ca atom displayed a largest positive charge, indicating electron donation from the Ca atom. Therefore, the Ca site can be effectively activated for O_2 adsorption on the doped surface. As following, analysis of partial density of states (PDOS) was then completed, which can provide additional insights and explanations for the electronic structure of the different doped configurations.

Our computed PDOS for each analyzed configuration is shown in Fig. 3. The corresponding maps divided into three regions: I, II, and III. Region I is the C, Be, Si, and B four doping configurations, region II is the Ge doping configuration, and region III is the Mg, Ca, and Ga three doping configurations. For all doped surfaces, it can be seen from Fig. 3 that the Al 3s-orbitals primarily dominate the valence band while the Al 3p-orbitals do in the conduction band. By comparison, contribution of the doped atoms to these bands is relatively small, but nevertheless exhibit some intriguing features. As illustrated in Fig. 3I(a), in the Be-doped surface the Be 2s-, 2p-orbitals have an obvious PDOS contribution in the conduction band, showing their ability of accept electrons. Moreover, in the energy range of -9 to -3 eV, the prominent overlap between the Be 2s-, 2p-orbitals proposes their strong orbital-hybridization. In contrast, PDOS of the B-doped surface differs from that of the Be-doped surface. Fig. 3I(b) shows that the B 2p contributes greatly to the valence band around Fermi level, unlike its 2 s orbital, which is in the low energy region with an energy range of -11 to -9 eV. This suggests that the doped B-atom also serves as an active site. Of course, the B atom can also accept electrons due to its 2p-orbital contribution in the conduction band. Interestingly, for the PDOS of the C-doped surface, as seen from Fig. 3I(c), unlike the Be- and B-doped examples mentioned above, the C 2s-orbital contributes minimally to the both bands, whereas its 2p-orbital electrons do significantly at approximately -6 eV. This further supports the conclusion that the C-atom should has less impact on the stability of the Al (111) surface. In the Si-doped surface, PDOS of the doped Si-atom is identical to that of the doped B-atom, with the exception that the Si 3p peak is almost equal in the both bands near Fermi level. This result can explains why the Si atom can acts as an O-adsorption site on the Si-doped surface, which will be discussed below. Overall, the orbitals of the four doped atoms, Be, B, Si, and C, contribute much less to the two bands than those of Al atoms, thereby providing more evidence for the doped-atoms permeating configurations. Fig. 3II (a) depicts PDOS of the Ge-doped configuration. An inspection of the Ge 4s-orbital reveals a noticeable Ge 4s concentration in the high energy region (2 to 6 eV). Moreover, the peaks of the Ge 4s-, 4p-orbitals overlap each other in the energy range of 3 to 6 eV, facilitating formation of the sp-hybrid empty orbitals. The doped Ga-atom has a very similar PDOS curves to the doped Ge-atom, as seen in Fig. 3II (a) and Fig. 3II (a). However, the Ga atom protrudes somewhat over the Ga-doped surface, presumably due to the larger atomic radius for Ga than Al. This conclusion can be confirmed by the results observed from both Mg- and Ca-doped surfaces, as illustrated in Fig. 1. It should be noted that peaks of the p-orbitals of the Mg and Ca atoms share a similar characteristic, where they overlap with the Al 3s-orbitals on the right side of Fermi level, as shown in Fig. 3III (a) and (b). However, the Ca atom can provide a 3d-orbital, in which its peak passes through Fermi energy and contributes significantly to the conduction band. Thus, contribution of the Ca 3d-orbital competes with that of the Al 3p-orbital,

weakening ability of O_2 adsorption on the Ca-doped surface. In addition, the Mulliken charge transfer analysis listed in Table 2 clearly shows that the Al atoms have a tendency to donate electrons to the Be, B, Ga, C, Si, and Ge atoms, so these doped atoms act as electron acceptor, in which the net charges increase 0.34 (Be), 1.01 (B), 0.04 (Ga), 1.25 (C), 0.21 (Si), and 0.07 (Ge) e, respectively. Notably, the C atom accepts the highest charge of 1.25 e, followed by the B atom with 1.01 e. These findings reflect the strong interactions between Al atoms and C and B atoms, at the same time this is key reason why the C and B atoms to permeate prominently in their configurations. This also further supports the strongest permeating propensity of the C atom in the C-doped surface. It is known that the Mg and Ca atoms have lower electronegativity than Al atom, which allows for easier electrons transfer from Mg and Ca atoms to the adjacent Al atoms. Our calculations show that the Mg and Ca atoms have a charge depletion of 0.74 and 0.75 e, respectively, resulting in them protruding from the surface of the Al material.

3.2. Adsorption of O_2 molecules

In this part, we compare the O_2 adsorption onto a pure Al (111) surface and onto surfaces where one dopant atom of the following elements was added, Be, Mg, Ca, B, Ga, C, Si, and Ge, and predict the effect of the doped atoms on the adsorption. With regard to the O_2 adsorption of the surfaces, as shown in Fig. 4, only in the Ca-doped configuration the O_2 exhibits a distance from the surface of 2.5 Å, indicating weak intermolecular interaction. In contrast, no matter where O_2 is adsorbed, in the other doped configurations the O_2 are entirely dispersed over the surfaces, effectively achieving surface oxidation. This observation is in accordance with both experimental [47-49] and theoretical [47-51] reports, in which the molecular adsorption product of O_2 shows little stability and its dissociation is widely regarded as a stable product. Therefore, we shall focus on the latter case, emphasizing chemical adsorption, and discuss more. In one sense, our results will provide fundamental insights into O_2 dissociative adsorption on these doped surfaces.

3.2.1. Oxidized by up to three O_2 molecules

It can be seen from Fig. 4, the O-adsorption of the Be, Mg, B, Ga, C, and Ge doped Al (111) surfaces can be successively achieved by three O_2 molecules. Chemical interactions is the most important characteristic in the adsorption process. Analogous to the simulation method proposed by Zhang et al. for the O-adsorption on Al-Mg surfaces with O_2 [52], in this study an O_2 molecule was initially placed parallel to the surface normal and from the top of doping-atom by 2.5 Å distance. After full geometric optimization, it was discovered that the initially placed O_2 molecule spontaneously dissociates into two O atoms and adsorbs onto the doped surface, which is well agreed with previous research findings [53]. Subsequently, analogous construction and optimization operation continue to carry out based on the configurations after optimization. However, for the Mg-doped configuration, the third placed O_2 displays an especial oxidation behavior after optimization, in which the entire O_2 molecule is attached to Mg atom and in parallel to the surface. This is strikingly similar to the reported pure Al example, [54] suggesting the oxide layer quickly converted into the familiar MgO at higher coverage. These results suggest the importance of the adsorption sites for the adsorption. In general, the surface site where the adsorbate adsorbs can emerge at three possible adsorption sites: top site, bridge site, and hollow site (hcp site and fcc site). In the next surface O-adsorption studies, according to characters of our calculated O-adsorption, we will mainly focus on two high-symmetry sites: fcc and hcp (collectively called hollow site), and by marked in Fig. 4(a), in which the fcc site was located in the center of the triangular facets produced by three surface atoms while the hcp site was directly above the atoms in the second layer of the Al substrate. Overall speaking as depicted in Fig. 4, the dissociated oxygen molecules are preferentially adsorbed onto the fcc or hcp sites nearest-neighbor doped-atom on the surface layer, which is analogous to

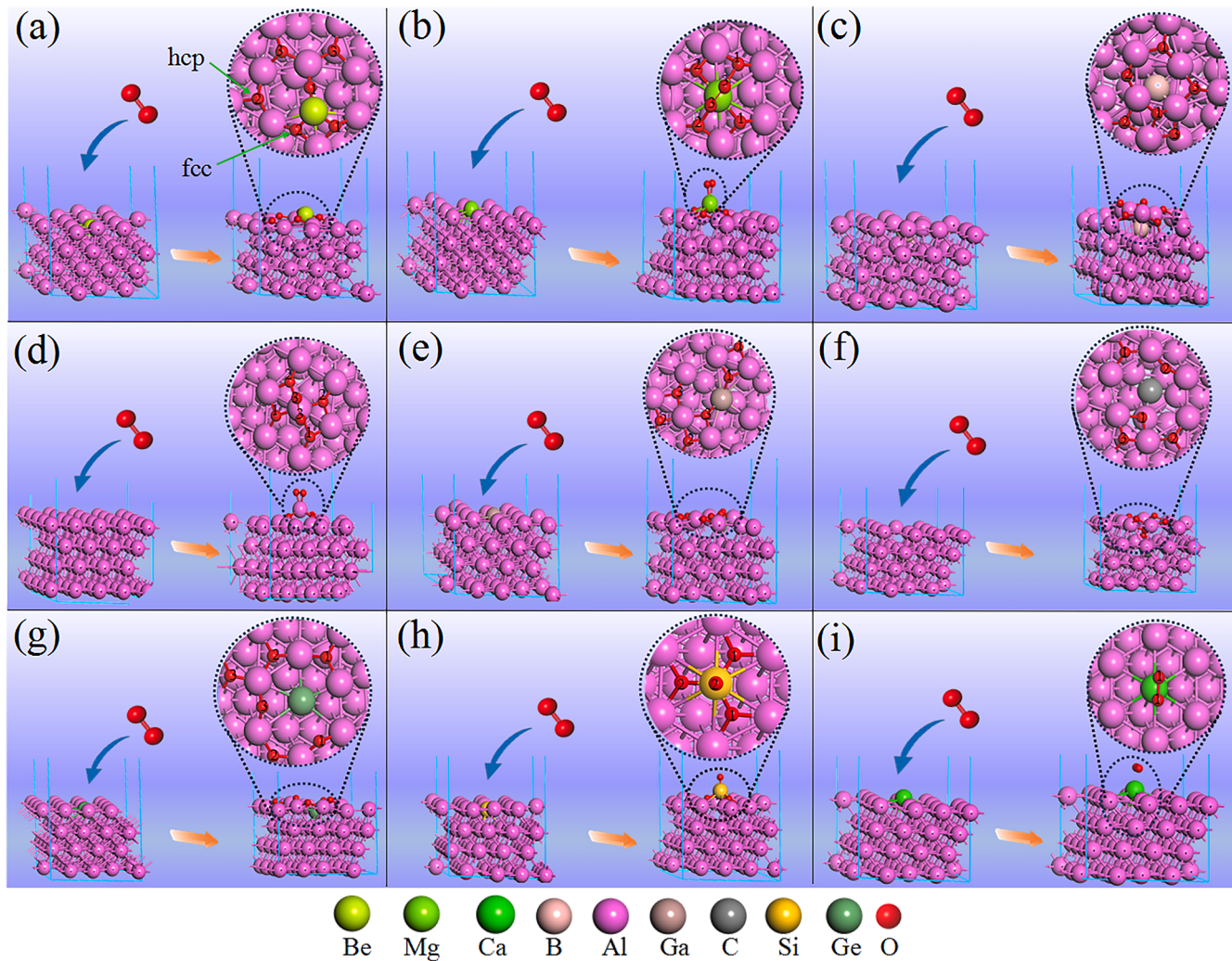


Fig. 4. Optimized configurations of O_2 adsorption on the pure and doped Al (111) surfaces. (a)-(g) represent three O_2 adsorption configurations, (h) represents two O_2 adsorption configuration, and (i) represents one O_2 adsorption configuration. As an example Fig. 4(a) depicts hcp and fcc sites of O_2 adsorption. The fcc (face-centered cubic) sites are found in the center of each triangular facet produced by three surface atoms, whereas the hcp (hexagonal close-packed) sites lie right above the atoms in the Al substrate's second layer. Similar arrangements apply to the remaining configurations.

the findings of Li et al. [55]. It is noteworthy that the Be-doped surface contains one bridge oxygen on the Be-Al bond in addition to some fcc or hcp oxygens. This bridge oxygen also appears on the B-, C-, and Ga-doped surfaces, but exclusively on the Al-Al bonds. Furthermore, comparing the position of the covered O-atoms on the doped surfaces reveals a higher concentration on the Mg-doped surface and a greater dispersion on the Ge-doped surface, with the Mg-doping covering the same area as the pure Al case. Nevertheless, the O-Al bonding dominated the O-adsorption, which is in good agreement with experimental reports

[43]. Table 3 presents the adsorption energies (E_{ads}) for all the adsorption configurations with various doping atoms. It can be found that the O-adsorption ability grows with increase in the quantity of adsorbed O_2 molecules, is concordant with the Long et al.'s [22]. This result infers that the increased O_2 molecular coverage aids the oxidation of the Al alloy surface. However, an excessive thick oxide layer can less favor the oxidation of the alloy surface. According to Baran et al. reported results [56], when the thickness of the oxide film on the Al surface increases, the E_{ads} value of O_2 gradually increases until it reaches zero. Additionally, with an increasing amount of the adsorbed O_2 molecules, there is a vary difference in our E_{ads} values as shown in Table 3. When only one O_2 molecule is adsorbed, the adsorption energy value (E_{ads1}) of the Be/Al is the smallest, ~ -10.43 eV. In contrast, the E_{ads1} values (eV) of the Mg/Al (-10.01), B/Al (-9.42), C/Al (-9.28), Ga/Al (-8.82), and Ge/Al (-8.52) are all higher than that of the pure Al (-10.03). It is worth noting that Dong et al. [3], through investigation of the O_2 adsorption on the Al (111) surfaces, proposed the E_{ads} values of -7.52 eV for the O atom at the fcc site and -7.21 eV for the O atom at the hcp site. Consequently, the E_{ads} of O_2 on the doped Al (111) surface configuration may be influenced not only by the intrinsic properties of the doped atoms, but also by an increase in the number of O-atoms occupying fcc adsorption sites. However, Qiao et al. [26] reported an E_{ads} value of -3.573 eV from their studied O_2 adsorption on the pure Al (111)

Table 3
Adsorption energy (E_{ads} , eV) of oxygen on the doped surfaces.^a

Species	E_{ads1}	E_{ads2}	E_{ads3}
Be/Al	-10.43	-20.erro37	-30.25
Mg/Al	-10.01	-19.70	-21.20
Ca/Al	-2.29	—	—
B/Al	-9.42	-20.27	-30.47
Ga/Al	-8.82	-18.72	-28.03
C/Al	-9.28	-19.11	-29.42
Si/Al	-8.93	-17.63	—
Ge/Al	-8.52	-19.03	-29.13
pure Al	-10.03	-19.65	-22.16

^a “—” indicates that can be inability to adsorb O_2 molecule.

surface. It is speculated that this is related to their selected calculation method with the GGA/PW91 functional that was used to describe the exchange-correlation energies. In contrast, our current computation, which employs the GGA/PBE functional, obtains an E_{ads} value of -10.03 eV for the $E_{\text{ads}1}$ of the pure Al surface, nearly aligning with the experimental value of -11.11 eV [57]. Based on these findings, we conclude that the GGA/PBE functional used in this work accurately predicts the occurrence of O₂ adsorption investigated here. Furthermore, once two O₂ molecules are adsorbed, the $E_{\text{ads}2}$ values (eV) of the Be/Al (-20.37), B/Al (-20.27), and Mg/Al (-19.70) become all smaller than that of the pure Al (-19.65), however, the corresponding values for the C/Al (-19.11), Ge/Al (-19.03), and Ga/Al (-18.72) increase. After three O₂

molecules are adsorbed, only Mg/Al (-21.20 eV) $E_{\text{ads}3}$ value increases while the $E_{\text{ads}3}$ (eV) value of the B/Al (-30.47), Be/Al (-30.25), C/Al (-29.42), Ge/Al (-29.13), and Ga/Al (-28.03) are all lower than that of the pure Al (-22.16). Obviously, the O-adsorption behavior of the Mg-doped Al surface is unstable, presumably due to excessive aggregation of the covered O-atoms.

The PDOS of the maximum O₂ adsorption on the Be-, Mg-, B-, Ga-, C-, and Ge-doped and clean Al (111) surfaces is collected in Fig. 5. The PDOS of the less than maximum O₂ adsorption configurations shown in FIGS. 4 and 5 (see the supplementary material). The maximum O₂ adsorption configurations were selected to analyze their electronic structure. Inspection of Fig. 5 displayed that after the O₂ molecules cover

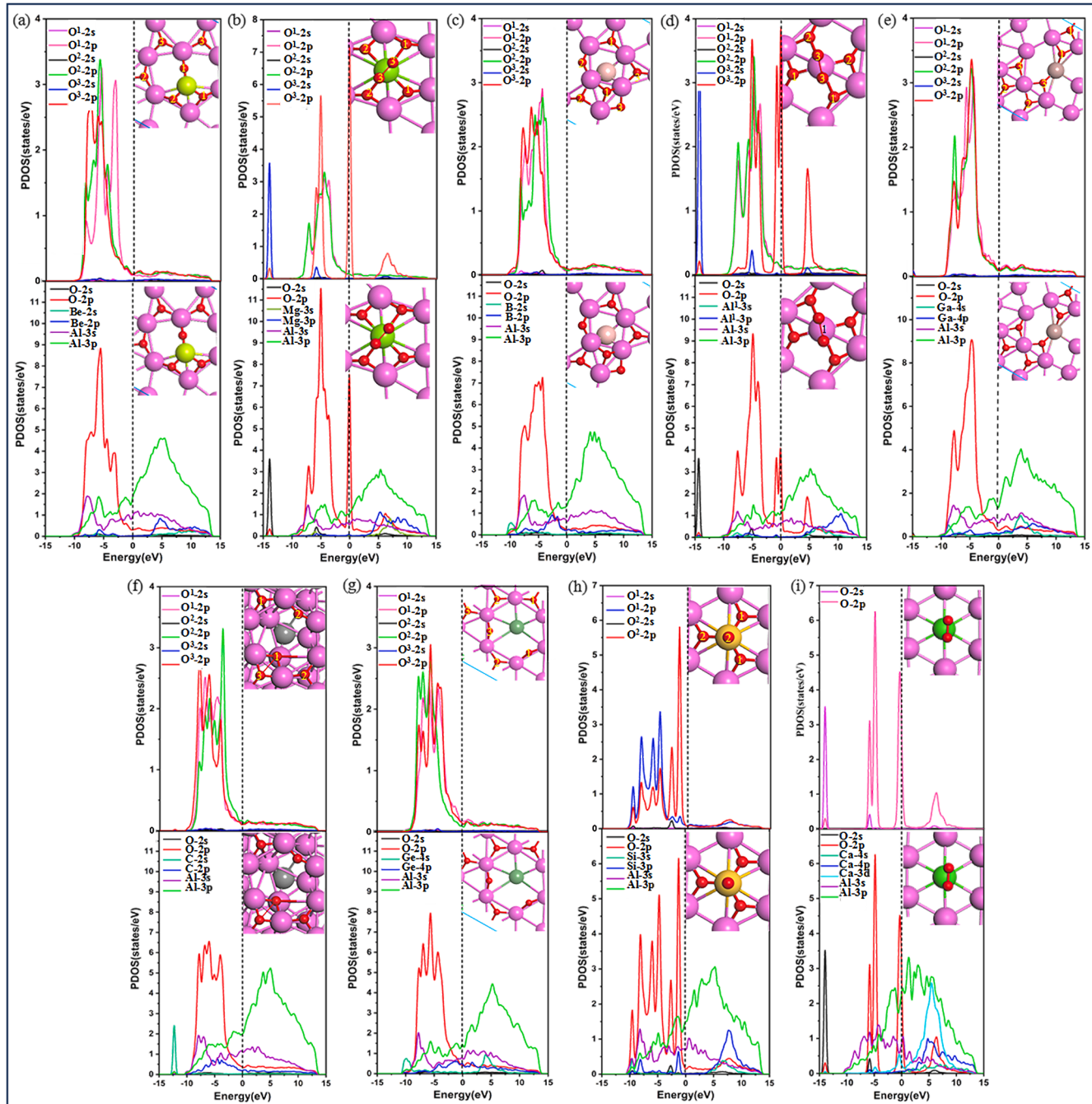


Fig. 5. PDOS of the O₂ adsorption on the pure and doped Al (111) surfaces. Adsorption of three O₂ for the Be/Al (a), Mg/Al (b), B/Al (c), pure Al (d), Ga/Al (e), C/Al (f), and Ge/Al (g) systems (the corresponding one and two O₂ examples shown in FIGS. 4 and 5 of Supporting Material). Adsorption of two O₂ for the Si/Al (h) system (the corresponding one O₂ examples presented in FIG. 4 of Supporting Material). Adsorption of one O₂ for the Ca/Al (i) system.

on the surfaces, the Al atoms' orbitals, rather than the doped atoms' orbitals, show significant overlap with the O 2p-orbitals. This overlap, which occurs in the energy range of -10 to -2 eV, involves the Al 3s-, 3p-orbitals. This result indicate that Al atom has a strong electron orbital interaction with O atoms, and this is also consistent with our binding energy analysis. Meanwhile, it was also found that contribution of the 2p-orbitals of the third absorbed O_2 molecule on the Mg-doped and pure Al surfaces all showing a significant increase at the Fermi energy, which derives from the O_2 absorption in molecular form. In addition the obvious observations, Fig. 5 also shows that after the O-adsorption, an interaction happens at the O-Al, where some electrons are transferred from the Al atom to the O atom. This, in turn, causes the Al atom's remaining electrons to move to a lower energy level, improves the bonding between the inner atoms in the Al surface, and ultimately displays the effect on the value of the binding energy. Additionally, as illustrated in Fig. 5(a), in the Be doped system, there is the increase of PDOS from 3 to 14 eV, which is mainly contributed by the Be atom 2p-orbital, the O atom 2p-orbital, and the Al atom 3s-orbital. In contrast, for the Mg doped system shown in Fig. 5(b), in the same energy range the large overlapped area exists between Mg 3 s, 3p, O 2p, and Al 3 s, respectively. Within this energy range, for both Ga- and Ge-doped configurations, the results are similar, which exhibit a comparable electrons distribution to the Mg-doped configuration. However, for the B- and C-doped configurations, as depicted by Fig. 5(c) together with Fig. 5(f), there is an obvious PDOS that shifted towards valence band near Fermi level, showing the large overlapped area between the doped atoms p-orbitals and Al atom 3s-orbitals. Especially, an obvious peak acutely locate at ~ -13 eV, which mainly reflects contribution of the C 2 s of the C-doped configuration, implying the severe permeating of C atom on its surface. The electron density difference (EDD) analysis, as shown in Fig. 6, indicates that during the O_2 adsorption on these surfaces, the absorbed O atoms will gain a significant number of electrons from the studied surfaces, at the same time there are also some electrons depletions due to the obvious contribution of the O 2p-orbitals near the Fermi level. It is not only proved that the strong electrons exchange between the O atoms and pure/doped Al surfaces but also inferred a chemical adsorption was occurred.

3.2.2. Oxidized by up to two O_2 molecules

This section investigates effect of the doped Si atom on the O-adsorption of the Al (111) surface. Our calculations show that the Si-doped Al (111) surface can be oxidized by up to two oxygen molecules. Initially, molecular axis of the placed O_2 molecule is parallel to the surface normal and hangs over the top of the Si site. After geometric optimization, the placed O_2 has completely dissociated and is more likely to be adsorbed at the top and hcp sites rather than the fcc site, as

seen in Fig. 4(h), where the three O atoms were attached to the hcp site near the Si atom, with just one O atom on the top. The computed E_{ads} values for the O atoms are presented in Table 3. From Table 3, it can be seen that E_{ads1} (-8.93 eV) and E_{ads2} (-17.63 eV) imply stable oxygen adsorption on the Si-doped Al (111) surfaces, with a preference for the hcp site over the top site, which is confirmed by prior reports [3,58]. Meanwhile, it is also discovered that the second O_2 is more easily adsorbed than the first one due to the more electron transfer from the original adsorbed-O atoms to the Si atom. Thus, as the adsorption process a Si-O chemical bond may be formed in the dissociated O atom and the base material. The calculated PDOS of the Si/Al configuration with O_2 adsorption illustrates a new peak in the energy range of -2 to 0 eV corresponded to the Si 3p orbital, as shown in Fig. 5(h), and there exists an obvious overlap with the O 2p orbital. Obviously, the overlapped area between Si 3p and O 2p can not only indicate that their orbits are highly hybridized, but also promote strong covalent bonding between the Si and O atoms through electron "donation/back-donation" interaction. Notably, the bonding state is below the Fermi level, suggesting that electrons go from the filled O-2p orbital to the empty π^* state of the Si-Al bond. Furthermore, when a second O_2 molecule oxidizes the Si/Al surface, the O-2p orbital near the Fermi level contributes considerably, making it difficult to accept more O_2 at these sites. Additionally, the EDD map presented in Fig. 6 provides the evidence for the charges depletion on the Si atom and the charges accumulation on the O atoms. Under this result, in addition to the formation of Al-O bonds, there is a strong interaction between O atom and Si atom on the Si-doped Al (111) surface.

4. Conclusions

In conclusion, this study utilizes DFT-GGA/PBE density functional to investigate Al alloy materials substituted with eight metals (Be, Mg, Ca, B, Ga, C, Si, and Ge) in the form of single atom on the Al (111) surface. As a performance test, we looked at their corresponding O_2 adsorption. The findings are as follows: (1) The investigated doping atoms can establish stable bonds with Al atoms on the Al (111) surface. The flatness of the doped surface is determined by the radius and electronic properties of the doping atoms. (2) O_2 molecules can spontaneously dissociate and adsorb onto the pure/doped Al (111) surfaces but the mechanism not on the Ca-doped Al (111) surface, where O_2 is adsorbed in molecular form. The amount of O-adsorption is correlated to the surface dopant atoms. (3) The surface site where the O atoms adsorb can emerge at four possible adsorption sites: top site, bridge site, hcp site and fcc site (collectively called hollow site), and the adsorption occurs preferentially at the hollow site. (4) Oxygen adsorption on the doped Al (111) surfaces rises along with O_2 coverage. It is expected that higher O_2 coverage will

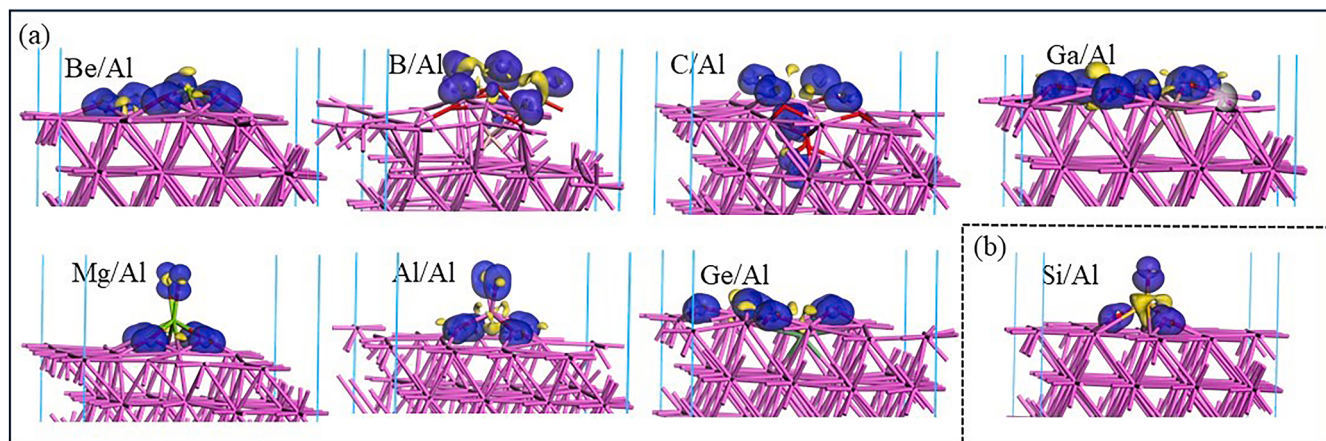


Fig. 6. Electron density difference (EDD) for the O_2 adsorption on the pure and doped Al (111) surfaces. Region (a) corresponds to the EDD of three O_2 adsorptions, while region (b) refers to the EDD of two O_2 adsorptions. The yellow and blue regions represent charge depletion and accumulation, respectively.

promote O₂ adsorption on the doped surface.

CRediT authorship contribution statement

Liang Junxi: Writing – review & editing, Validation, Supervision, Resources. **Qi Bomiao:** Writing – original draft, Software, Investigation. **Lu Mengmeng:** Software, Resources. **Zhou Yaoyu:** Software, Resources. **Ren Fang:** Formal analysis. **Shen Yan:** Software, Resources. **Li Guihua:** Software, Resources. **Pang Shaofeng:** Software, Resources. **Wang Yanbin:** Software, Resources. **Su Qiong:** Writing – review & editing, Software, Resources.

Declaration of competing interest

The author has no conflict of interest.

Data availability

Data will be made available on request.

Acknowledgments

The authors are thankful to Lu Zhibin (Chinese Acad Sci, Lanzhou Inst Chem Phys, State Key Lab Solid Lubricat) for technical assistance.

Supplementary materials

Supplementary material associated with this article can be found, in the online version, at doi:10.1016/j.surfin.2024.105075.

References

- [1] J.V.S. Araujo, M. Milagre, I. Costa, A historical, statistical and electrochemical approach on the effect of microstructure in the anodizing of Al alloys: a review, *Crit. Rev. Solid State* (2023) 1–61.
- [2] S. Jin, J.D. Head, Theoretical investigation of molecular water adsorption on the Al (111) surface, *Surf. Sci.* 318 (1994) 204–216.
- [3] X. Wei, C. Dong, Z. Chen, K. Xiao, X. Li, A DFT study of the adsorption of O₂ and H₂O on Al (111) surface, *RSC Adv* 6 (2016) 56303–56312.
- [4] F. Cao, H. Cui, X. Song, L. Gao, M. Liu, Q. Qiao, H. Kong, Fabrication of multiscale TiC and stainless steel composite coatings via circular oscillating laser towards superior wear and corrosion resistance of aluminum alloy, *J. Mater. Sci. Technol.* 177 (2024) 191–204.
- [5] J. Li, T. Yuan, C. Zhou, B. Chen, Y. Shuai, D. Wu, D. Chen, X. Luo, Y.F. Cheng, Y. Liu, Facile Li-Al layered double hydroxide films on Al alloy for enhanced hydrophobicity, anti-biofouling and anti-corrosion performance, *J. Mater. Sci. Technol.* 79 (2021) 230–242.
- [6] J. Chen, Z. He, J. Liu, Y. Wang, M. Hodgson, W. Gao, Antibacterial anodic aluminium oxide-copper coatings on aluminum alloys: preparation and long-term antibacterial performance, *Chem. Eng. J.* 461 (2023) 141873.
- [7] F. Mollaamin, M. Monajjemi, Molecular modelling framework of metal-organic clusters for conserving surfaces: langmuir sorption through the TD-DFT/ONIOM approach, *Mol. Simulat.* 49 (2023) 365–376.
- [8] F. Mollaamin, M. Monajjemi, Molecular simulation of (Al-Ga) urface garnished with chromium metal for organic material detecting: a DFT study, *Funct. Mater. Lett.* 16 (2023) 2340028.
- [9] F. Mollaamin, M. Monajjemi, In silico-DFT investigation of nanocluster alloys of Al-(Mg, Ge, Sn) coated by nitrogen heterocyclic carbenes as corrosion inhibitors, *J. Clust. Sci.* 34 (2023) 2901–2918.
- [10] F. Mollaamin, S. Shahriari, M. Monajjemi Z. Khalaj, Nanocluster of aluminum lattice via organic inhibitors coating: a study of freundlich adsorption, *J. Clust. Sci.* 34 (2023) 1547–1562.
- [11] Q. Cai, C.L. Mendis, S. Wang, I.T.H. Chang, Z. Fan, Effect of heat treatment on microstructure and tensile properties of die-cast Al-Cu-Si-Mg alloys, *J. Alloys Compd.* 881 (2021) 160559.
- [12] S.J. Kang, Y.W. Kim, M. Kim, J.M. Zuo, Determination of interfacial atomic structure, misfits and energetics of X phase in Al-Cu-Mg-Ag alloy, *Acta Mater.* 81 (2014) 501–511.
- [13] Q. Cai, C.L. Mendis, I.T.H. Chang, Z. Fan, Microstructure and mechanical properties of new die-cast quaternary Al-Cu-Si-Mg alloys, *Mater. Sci. Eng. A* 800 (2021) 140357.
- [14] M. Souissi, C.M. Fang, R. Sahara, Z. Fan, Formation energies of θ -Al₂Cu phase and precursor Al-Cu compounds: importance of on-site coulomb repulsion, *Comput. Mater. Sci.* 194 (2021) 110461.
- [15] Z.Q. Zheng, W.Q. Liu, Z.Q. Liao, S.P. Ringer, G. Sha, Solute clustering and solute nanostructures in an Al-3.5Cu-0.4Mg-0.2Ge alloy, *Acta Mater.* 61 (2013) 3724–3734.
- [16] Y. Chen, Q. Hu, S. Pan, H. Zhang, H. Liu, B. Zhu, X. Liu, W. Liu, Influences of Cu content on the microstructure and strengthening mechanisms of Al-Mg-Si-xCu alloys, *Metals* 9 (2019) 524.
- [17] C. Fang, M. Souissi, Z. Que, Z. Fan, Crystal chemistry and electronic properties of the Al-rich compounds, Al₂Cu, α -Al₂Cu₂Fe and θ -Al₁₃Fe₄ with Cu solution, *Metals* 12 (2022) 329.
- [18] H.K. Kamga, D. Larouche, M. Bourrane, A. Rahem, Mechanical properties of aluminum-copper B206 alloys with iron and silicon additions, *Int. J. Cast Metal. Res.* 25 (2012) 15–25.
- [19] Z. Chen, J. Zhang, J. Shu, G. Sha, J. Xia, S. Wang, S.P. Ringer, Effects of Si addition on the microstructure evolution of Al-Cu-Mg alloys in the α + S + T phase field, *Philos. Mag. Lett.* 93 (2013) 648–654.
- [20] C. Li, G. Sha, B. Guo, J.H. Xia, X.F. Liu, Y.Y. Wu, N. Birbilis, S.P. Ringer, Enhanced age-hardening response of Al-4Mg-1Cu (wt.%) micro-alloyed with Ag and Si, *Scr. Mater.* 68 (2013) 857–860.
- [21] D. Costa, T. Ribeiro, F. Mercuri, G. Pacchioni, P. Marcus, Atomistic modeling of corrosion resistance: a first principles study of O₂ reduction on the Al (111) surface covered with a thin hydroxylated alumina film, *Adv. Mater. Interfaces* 1 (2014) 1300072.
- [22] F.Y. Guo, C.G. Long, J. Zhang, Z. Zhang, C.H. Liu, K. Yu, Adsorption and dissociation of H₂O on Al (111) surface by density functional theory calculation, *Appl. Surf. Sci.* 324 (2015) 584–589.
- [23] A. Akçak, A.E. Genc, B. Kutlu, BH₄ dissociation on various metal (111) surfaces: a DFT study, *Appl. Surf. Sci.* 473 (2019) 681–692.
- [24] Y. Kim, J. Choi, Oxide growth characteristics on Al (100), (110), and (111) surfaces: a chemo-mechanical evaluation, *Mater. Today Commun* 26 (2021) 102006.
- [25] N. Cai, G. Zhou, K. Müller, D.E. Starr, Effect of oxygen gas pressure on the kinetics of alumina film growth during the oxidation of Al (111) at room temperature, *Phys. Rev. B* 84 (2011) 125445.
- [26] Y. Qiao, L. Xu, H. Zhang, H. Luo, O₂ dissociative adsorption on the Cu-, Ag-, and W-doped Al (111) surfaces from DFT computation, *Surf. Interface Anal.* 53 (2021) 46–52.
- [27] H. Ji, K. Ren, J. Yang, Y. Zhang, G. Wang, Effects of Zn, Mg and Cu doping on oxidation reaction of Al (111) surface, *Front. Chem.* 10 (2022) 930900.
- [28] F. Mollaamin, M. Monajjemi, Transition metal (X= Mn, Fe, Co, Ni, Cu, Zn)-doped graphene as gas sensor for CO₂ and NO₂ detection: a molecular modeling framework by DFT perspective, *J. Mol. Model.* 29 (2023) 119.
- [29] F. Mollaamin, M. Monajjemi, The influence of Sc, Cr V, Cu Co, Zn as ferromagnetic semiconductors implanted on B₅N₁₀-nanocarrier for enhancing of NO sensing: an environmental eco-friendly investigation, *Comput. Theor. Chem.* 1237 (2024) 114666.
- [30] Accelrys Inc., Materials studio version 8.0, Accelrys Inc.: San Diego, CA, USA, 2014.
- [31] X. Zhang, D. Chen, H. Cui, X. Dong, S. Xiao, J. Tang, Understanding of SF₆ decompositions adsorbed on cobalt-doped SWCNT: a DFT study, *Appl. Surf. Sci.* 420 (2017) 371–382.
- [32] J. Zhang, R. Zhang, B. Wang, L. Ling, Insight into the adsorption and dissociation of water over different CuO (111) surfaces: the effect of surface structures, *Appl. Surf. Sci.* 364 (2016) 758–768.
- [33] W. Wang, L. Fan, G. Wang, Carbon disulfide (CS₂) adsorption and dissociation on the Cu (100) surface: a quantum chemical study, *Appl. Surf. Sci.* 414 (2017) 92–100.
- [34] J. Liu, S. Wen, J. Deng, X. Chen, Q. Feng, DFT study of ethyl xanthate interaction with sphalerite (110) surface in the absence and presence of copper, *Appl. Surf. Sci.* 311 (2014) 258–263.
- [35] S. Hou, D. Fang, Q. Jin, Y. Ye, Q. Li, F. He, J. Xie, First principle study on the interactions of NH₃, NO_x and O₂ with Fe₃O₄ (111) surfaces, *Appl. Surf. Sci.* 605 (2022) 154645.
- [36] A.T. Dinsdale, SGTE data for pure elements, Calphad 15 (1991) 317–425.
- [37] C.H. Zhang, J.J. Han, S.O. Huang, J. Shen, Chen's lattice inversion embedded-atom method for Fcc metal, *Adv. Mater. Res.* 320 (2011) 415–420.
- [38] Y. Liu, S. Zhang, R. Gou, Q. Huang, Z. Jiang, M. Chen, H. Gao, Density functional calculations of the adsorption and decomposition of RDX-AP on Al (1 1 1) surface, *Comput. Theor. Chem.* 1167 (2019) 112604.
- [39] H.J. Monkhorst, J.D. Pack, Special points for brillouin-zone integrations, *Phys. Rev. B* 13 (1976) 5188–5192.
- [40] L.A. Burns, A.V. Mayagoitia, B.G. Sumpter, C.D. Sherrill, Density-functional approaches to noncovalent interactions: a comparison of dispersion corrections (DFTD), exchange-hole dipole moment (XDM) theory, and specialized functionals, *J. Chem. Phys.* 134 (2011) 084107.
- [41] K. Fukushima, H. Esaki, Theoretical study of the mechanism of ribosomal peptide bond formation using the ONIOM method, *Chem. Pharm. Bull.* 69 (2021) 734–740.
- [42] E. Zuo, X. Dou, Y. Chen, W. Zhu, G. Jiang, A. Mao, J. Du, Electronic work function, surface energy and electronic properties of binary Mg-Y and Mg-Al alloys: a DFT study, *Surf. Sci.* 712 (2021) 121880.
- [43] L. Wang, J.X. Shang, F.H. Wang, Y. Chen, Y. Zhang, Oxygen adsorption on γ -TiAl surfaces and the related surface phase diagrams: a density-functional theory study, *Acta Mater.* 61 (2013) 1726–1738.
- [44] P. Blöński, A. Kiejna, J. Hafner, Theoretical study of oxygen adsorption at the Fe (110) and (100) surfaces, *Surf. Sci.* 590 (2005) 88–100.
- [45] X. Zhang, Z. Cui, L. Yi, Y. Li, H. Xiao, D. Chen, Theoretical study of the interaction of SF₆ molecule on Ag (111) surfaces: a DFT study, *Appl. Surf. Sci.* 457 (2018) 745–751.

- [46] L. Vitos, A.V. Ruban, H.L. Skriver, J. Kollár, The surface energy of metals, *Surf. Sci.* 411 (1998) 186–202.
- [47] I.P. Batra, L. Kleinman, Chemisorption of oxygen on aluminum surfaces, *J. Electron Spectrosc. Relat. Phenom.* 33 (1984) 175–241.
- [48] J. Trost, H. Brune, J. Winterlin, R.J. Behm, G. Ertl, Interaction of oxygen with Al (111) at elevated temperatures, *J. Chem. Phys.* 108 (1998) 1740–1747.
- [49] H. Brune, J. Winterlin, R.J. Behm, G. Ertl, Surface migration of “hot” adatoms in the course of dissociative chemisorption of oxygen on Al(111), *Phys. Rev. Lett.* 68 (1992) 624–626.
- [50] Y. Yourdshahyan, B. Razaznejad, B.I. Lundqvist, Adiabatic potential-energy surfaces for oxygen on Al (111), *Phys. Rev. B* 65 (2002) 075416.
- [51] Y.F. Zhukovskii, P.W.M. Jacobs, M. Causá, On the mechanism of the interaction between oxygen and close-packed single-crystal aluminum surfaces, *J. Phys. Chem. Solids* 64 (2003) 1317–1331.
- [52] F. Zhang, S. Zhu, Y. Teng, First-principles studies of the adsorption of O₂ on Al (001), *Chinese Sci. Bull.* 49 (2004) 1768–1771.
- [53] N. Cai, G. Zhou, K. Müller, D.E. Starr, Effect of oxygen gas pressure on the kinetics of alumina film growth during the oxidation of Al (111) at room temperature, *Phys. Rev. B* 84 (2011) 125445.
- [54] A. Pashutski, A. Hoffman, M. Folman, Low temperature XPS and AES studies of O₂ adsorption on Al(100), *Surf. Sci. Lett.* 208 (1989) L91–L97.
- [55] H. Li, L.M. Liu, S.Q. Wang, H.Q. Ye, First-principles study of oxygen atom adsorption on γ -TiAl(111) surface, *Acta Metall. Sin.* 42 (2006) 897–902.
- [56] J.D. Baran, H. Grönbeck, A. Hellman, Mechanism for limiting thickness of thin oxide films on aluminum, *Phys. Rev. Lett.* 112 (2014) 146103.
- [57] C.M. Lousada, P.A. Korzhavyi, Oxygen adsorption onto pure and doped Al surfaces—the role of surface dopants, *Phys. Chem. Chem. Phys.* 17 (2015) 1667–1679.
- [58] R. Yin, Y. Zhang, F. Libisch, E.A. Carter, H. Guo, B. Jiang, Dissociative chemisorption of O₂ on Al (111): dynamics on a correlated wave-function-based potential energy surface, *J. Phys. Chem. Lett.* 9 (2018) 3271–3277.